

# Couplings of hybrid operators to ground and excited states of bottomonia

Tommy Burch, Christian Ehm ann

Institut für Theoretische Physik, Universität Regensburg, D-93040 Regensburg,  
Germany

---

## Abstract

We analyze the overlap of color-octet meson operators with the  $\psi$  and the  $\psi'$  and their excited states, especially the first radial excitations. Our analysis is based on NRQCD and includes all terms up to order  $v^4$ . We use a variety of source and sink operators as a basis for the variational method, which enables us to clearly separate the mass eigenstates and hence to extract the desired amplitudes. The results show the usefulness of the variational method for determining couplings to excited hadronic states.

Key words: Lattice gauge theory, hadronic structure

---

## 1 Introduction

The inner structure of hadrons is one of the most shrouded and difficult issues of modern physics. Due to the confining nature of strong interactions, perturbative QCD calculations cannot describe physics at hadronic energy scales from first principles. However, lattice QCD, as a nonperturbative approach, has succeeded in confirming and predicting properties of matter at these scales. Since a priori we are not very well versed in the structure of hadronic states, we try to probe them on the lattice with suitable operators. In quantum field theory, the only condition for non-zero overlap of an eigenstate of the underlying Hamiltonian with a specific operator is that the operator has the same quantum numbers as the mass eigenstate. So all physical states, the ground state as well as all its excitations, are expected to couple non-trivially to currents which project out the corresponding quantum numbers. A recent paper by Liu and Luo [1], addressed to spectroscopy of charmonia, suggests that there is an exception to this rule. In correlators, which they constructed from hybrid operators, no radial excitations are visible. Only the ground state and a much higher lying state, most probably a hybrid excitation, appear. We

want to check this result for bottomonium systems in the pseudoscalar and vector channel. Furthermore, we want to provide quantitative estimates for the couplings. To do so, we use the variational method, which is based on the construction of a cross correlator matrix. This approach enables us not only to investigate the spectrum, but more importantly, to obtain ratios of couplings of different local operators to a physical state. A similar approach was recently used for excited pions [2].

This paper is organized as follows. The purpose of Section 2 is to give a brief definition (in the heavy quark limit) of a hybrid excitation. Section 3 describes the variational method we use for extracting masses and couplings. Our implementation of the NRQCD framework to propagate the fermions is discussed in Section 4. Section 5 gives an overview of the configurations, on which we are running our simulation. The actual results are presented in Section 6 and Section 7 contains concluding remarks.

A preliminary report of these results can be found in [3].

## 2 Hybrids

In the heavy quark limit we can define a hybrid meson unambiguously: A hybrid is an excitation in a given channel with large contributions in which quark and antiquark form a color octet (and are therefore accompanied by an arbitrary number of valence gluons in order to obtain an overall singlet) as compared to the contributions in which the qq pair transform trivially in color space. It is needless to say that none of these states, which merely serve as an expanding basis for the hybrid, are physical in QCD, since mixing between them is possible. In the framework of NRQCD we can actually identify the terms in the Lagrangian, which are responsible for this, so called, configuration mixing. This has been studied in [4], for instance. Since such configuration mixings are ever-present in physical hadronic systems, all states should have overlap with hybrid operators, which project out the qq color-octet component.

## 3 Method

To gain information on the couplings we rely on the variational method. The starting point is the construction of a cross correlator matrix  $C_{ij}$ :

$$C_{ij}(t) = \langle 0 | \hat{\mathcal{O}}_i(t) \hat{\mathcal{O}}_j(0) | 0 \rangle \quad (1)$$

The operators  $\hat{O}_i$  we use will be specified below. Then we can solve the generalized eigenvalue problem

$$C_{ij}(t) \vec{v}_j^n = \lambda_n(t; t_0) C_{ij}(t_0) \vec{v}_j^n; \quad (2)$$

where  $\lambda_n$  is the eigenvalue corresponding to the eigenvector  $\vec{v}^n$ . Since, due to fluctuations,  $C_{ij}$  is not exactly symmetric (although it is within errors), we symmetrize it by hand in order to make the diagonalization procedure more stable.

The eigenvalues are then given by [6,7]

$$\lambda_n(t; t_0) = A_n e^{-M_n(t-t_0)} [1 + O(e^{-M_n(t-t_0)})]; \quad (3)$$

where  $M_n$  denotes the mass of the  $n$ th state and  $M_{n+1}$  the mass difference to the next state. This correction is due to the use of a finite number of operators in the basis. However, for large enough values of  $t$ , we have a single mass state in each channel. Thus, the variational method enables us to clearly separate the ground state, many lower lying excitations, and even ghosts [8] (which do not play any role in this work).

For our purposes here, even more important than the eigenvalues is the analysis of the eigenvectors. Consider the following ratio:

$$\frac{C_{ij}(t) \vec{v}_j^n}{C_{k1}(t) \vec{v}_1^n} = \frac{\langle \hat{O}_i \vec{v}_j^n | \hat{O}_j \vec{v}_i \rangle_{t, t_0}}{\langle \hat{O}_k \vec{v}_1^n | \hat{O}_1 \vec{v}_i \rangle_{t, t_0}} = \frac{\langle \hat{O}_i \vec{v}_j^n | \hat{O}_j \vec{v}_i \rangle}{\langle \hat{O}_k \vec{v}_1^n | \hat{O}_1 \vec{v}_i \rangle} = \frac{h_{ij}}{h_{k1}}; \quad (4)$$

where  $h_{ij}$  stands for the overlap of the  $i$ th operator with the  $n$ th eigenstate. Consequently, we are able to make statements about the ratios of couplings of different operators to the same state.

The success of the variational method strongly depends on the choice of operators one includes in the basis. Unfortunately, there will in any case only be a finite number of operators available, which can just span a subspace of the Hilbert space of states. Therefore, one tries to use operators which are "as linearly independent as possible"; i.e., they should have small relative overlap. Since we want to investigate the  $\rho$  and the  $\omega$ , we use pseudoscalar and vector currents. For both we have a "normal" and a "hybrid" version. Table 1 gives an overview of the local operators we use. The P-wave states are only needed to set the scale. In order to assemble our basis with more linearly independent operators, we additionally smear the quark and the anti-quark field independently with two different smearing levels (narrow and wide) using gauge invariant Jacobi smearing.

In total, twelve different operators, each at the source and the sink, are available for constructing the cross correlator matrix.

state	$J^{PC}$	normal operator	hybrid operator
b	$0^{-+}$	$\gamma$	$\gamma_i B_i$
	1	$\gamma_i$	$\gamma B_i$
b0	$0^{++}$	$\gamma_i D_i$	-
b1	$1^{++}$	$\gamma_{ijk} j D_k$	-
b2	$2^{++}$	$\gamma (i D_j + j D_i - \frac{2}{3} ij k D_k)$	-

Table 1

Overview of the used operators  $\hat{O}_i$ . The hybrid versions of the P-waves are not needed.

#### 4 NRQCD

The calculation of the propagators is performed in the framework of NRQCD [9], which is perfectly suitable for our bottomonium systems, where the quarks move with small velocities. We include all terms up to  $O(v^4)$  in our NRQCD Lagrangian, where  $v$  is the velocity of a quark, according to the power counting in [9]. Since we are working in a nonrelativistic approximation, the propagation of the fermions can be described by the quantum mechanical evolution operator for imaginary time  $e^{-Ht}$ . By expanding this operator we obtain for the propagation:

$$\langle \gamma; t+a \rangle = 1 - \frac{aH_0(t+a)}{2n} U_4^\gamma(t) - \frac{aH_0(t)}{2n} (1 - aH(t)) \langle \gamma; t \rangle; \quad (5)$$

where  $H_0$  is

$$H_0 = \frac{\tilde{\phantom{a}}}{2M} - \frac{a}{4n} \frac{\tilde{\phantom{a}}^2}{4M^2} \quad (6)$$

and  $H$  is

$$H = \frac{1}{8M^3} \tilde{\phantom{a}}^2 + \frac{ig}{8M^2} (\mathbf{r} \cdot \mathbf{E} \cdot \mathbf{E} \cdot \mathbf{r}) + \frac{g}{8M^2} (\tilde{\mathbf{r}} \cdot \mathbf{E} \cdot \mathbf{E} \cdot \tilde{\mathbf{r}}) + \frac{g}{2M} B; \quad (7)$$

The tildes denote improved versions of the corresponding derivatives. We use  $n = 2$ , which is more than sufficient in our case.  $B$  and  $E$  are the magnetic and electric fields created via the usual clover formulation. The last two terms of (7) are responsible for the configuration mixing mentioned above; however, it turns out that the  $B$  term produces a much larger effect.

To correct for tadpole contributions we divide each link by a factor  $u_0$  which is given by the fourth root of the average plaquette [10]. The quark mass for our simulation is determined from finite momentum correlators for the  $b$  by tuning the kinetic mass extracted from the non-relativistic energy-momentum dependence to the experimental mass of the  $b$ .

## 5 Configurations

We are working on configurations provided by the MILC-collaboration [11]. They were generated using improved staggered fermions and the Luscher-W eisz gauge action. Table 2 shows the parameters of the lattices used. For the lattice spacing, there are two values given. The first one comes from the analysis of the spin-averaged  $1P-1S$  splitting, the second one is given by the MILC-collaboration, where they used the improved Sommer parameter  $r_1$  to set the scale. Note that for the quenched lattice we are slightly above the values from the MILC-collaboration. This is most likely due to the wrong curvature of the  $qq$  potential in quenched simulations, thus influencing the  $P$ - and the  $S$ -waves differently.

To obtain the physical  $b$ -quark mass at the corresponding scales, we inter-/extrapolate to the experimental mass. However, both for the spectra and the ratios of the couplings, we find a very weak dependence upon the quark mass parameter.

	$a^{-1} [M eV]$	volume	$N_f$	$am_{sea}$	$am_b$	$m_b^{phys} [M eV]$	# of con gs.
8.40	2378 (7)/2279	$28^3 \cdot 96$	0	1	1.7, 1.8	4114 (72)	160
7.09	2097 (9)/2252	$28^3 \cdot 96$	$2+1$	0.0062/0.031	1.7, 1.8	4026 (65)	210
6.76	1495 (6)/1587	$20^3 \cdot 64$	$2+1$	0.01/0.05	2.4, 2.5	4111 (48)	410

Table 2

The three different lattices we use in our simulations together with the corresponding parameters. The first value for the inverse lattice spacing comes from the  $1P-1S$  splitting, the second one is given in [11].

## 6 Results

### 6.1 Spectra

At first we want to present the results for the masses in the considered channels. Table 3 gives some of the  $S$ -wave splittings for the quenched and dynamical lattices. Besides the hyperfine splitting in the dynamical case, all results agree with the experimental values, of course, only within the errors. Figure 1 shows the plot of the absolute masses. The fits are one exponential fits to the corresponding correlators of the states, using the full covariance matrix. For the pseudoscalar and the vector channel we use the variational method in the basis  $Nll, Nln, Nnn, Nww, Hll$ <sup>1</sup> and thus are able to obtain masses of their excited states reliably, the masses of the other states are extracted from single correlators. The absolute mass offset is fixed by the value of the  $m_b$ . For both types of configurations the quark mass parameter was set to  $am_b = 1.7$ . It is worth noting that the experimental input for the  $m_b$  comes from a single event, so it is not very reliable.

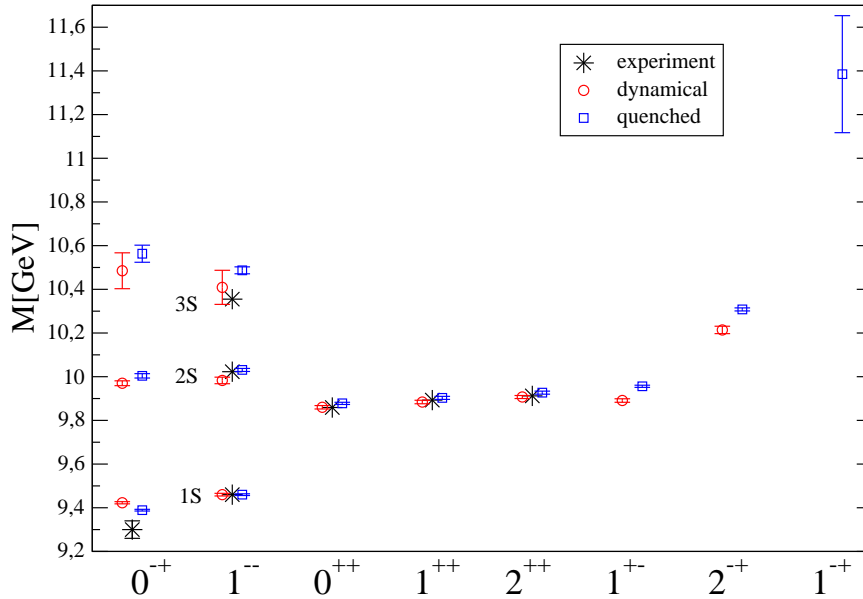


Fig. 1. Spectra of the available states, obtained by fitting the corresponding correlators, for both quenched ( $\beta = 8.40$ ) and dynamical configurations ( $\beta = 7.09$ ).

<sup>1</sup> The capital letter denotes the type of the operator:  $N$  = normal,  $H$  = hybrid; the two small ones give the smearing of the quark and the antiquark respectively:  $l$  = local,  $n$  = narrow,  $w$  = wide.

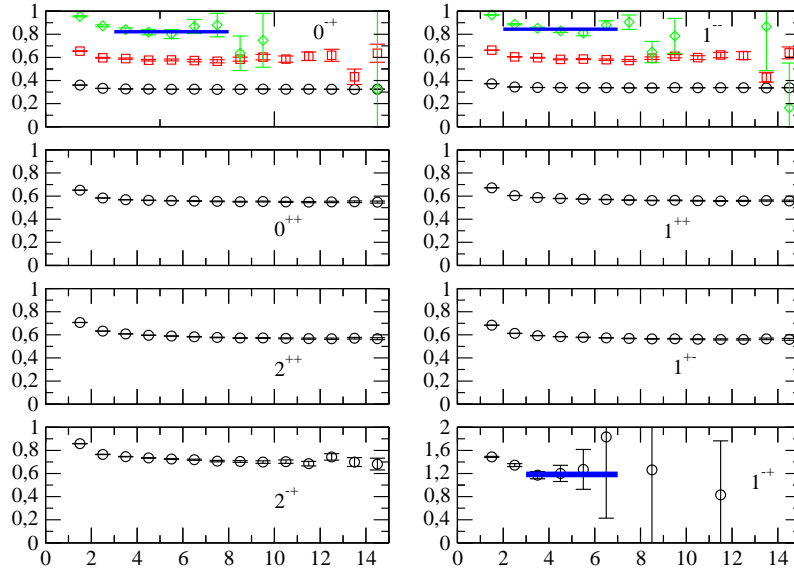


Fig. 2. Effective mass plots of the available states from the quenched lattice with  $\beta = 8.40$ .

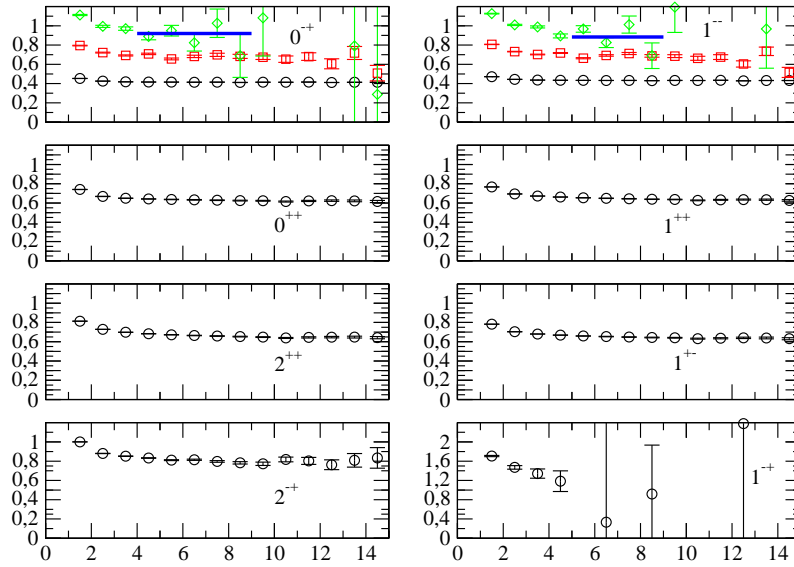


Fig. 3. Effective mass plots of the available states from the dynamical lattice with  $\beta = 7.09$ .

	0 <sup>+</sup> (1S)	0 <sup>+</sup> (2S)	0 <sup>+</sup> (3S)	1 <sup>-</sup> (1S)	1 <sup>-</sup> (2S)	1 <sup>-</sup> (3S)
experimental	9.300 (28)	-	-	9.460	10.023	10.355
quenched	9.389 (4)	10.004 (10)	10.563 (39)	9.460 (4)	10.031 (7)	10.487 (16)
$\chi^2$ =dof	2.49/5	7.42/4	2.50/4	6.76/5	2.36/4	5.64/4
t range	4-10	3-8	3-8	4-10	3-8	2-7
dynamical	9.423 (5)	9.970 (11)	10.485 (82)	9.460 (6)	9.983 (15)	10.409 (78)
$\chi^2$ =dof	4.56/5	6.56/5	2.43/4	2.65/4	1.71/3	1.27/3
t range	4-10	4-10	4-9	10-15	7-11	5-9
	0 <sup>++</sup>	1 <sup>++</sup>	2 <sup>++</sup>	1 <sup>+</sup>	2 <sup>+</sup>	1 <sup>+</sup>
experimental	9.859	9.893	9.912	-	-	-
quenched	9.878 (5)	9.903 (5)	9.927 (7)	9.956 (5)	10.308 (7)	11.385 (268)
$\chi^2$ =dof	2.79/5	4.52/4	2.44/2	5.89/5	8.03/7	0.74/2
t range	10-17	12-18	16-19	10-16	7-15	3-7
dynamical	9.860 (8)	9.884 (8)	9.907 (7)	9.891 (8)	10.214 (17)	-
$\chi^2$ =dof	3.15/4	5.09/4	3.04/4	3.02/3	4.63/4	-
t range	11-16	11-16	11-6	11-15	9-14	-

Table 3

Fitting results for the masses in GeV for both quenched ( $\beta = 8.40$ ) and dynamical configurations ( $\beta = 7.09$ ).

## 6.2 Starting basis

We proceed to the analysis of the eigenvalues and eigenvectors of the cross correlator matrix. As described above we construct the correlator matrix with a variety of source and sink operators and diagonalize it. By this procedure we hope to clearly separate the mass eigenstates and use the eigenvectors to shed light on their overlap with the included operators.

We start our analysis for the  $\beta$ , which is probably the experimentally more interesting state, on the dynamical lattice with  $\beta = 7.09$  and a quark mass parameter of  $am_b = 1.7$ . Later on we will also investigate the other lattices with different parameters to see what changes arise.

The smallest basis, including a hybrid operator, which reveals reasonable results, is  $N_{ll}(1)$ ,  $N_{nn}(2)$ ,  $H_{ll}(3)$ . The numbers in brackets are given just for the sake of clarity in the coupling ratio plots. The effective masses of the eigenstates are shown in Fig. 4. The ground state and the first radial excitation are clearly visible. For the first few time slices, the third eigenvalue may correspond to the hybrid excitation, due to its high mass.

To check if our diagonalization worked correctly, we can reconstruct the eigenvalue by multiplying the eigenvector with the cross correlator matrix  $C_{ij}(t) \begin{smallmatrix} n \\ j \end{smallmatrix}$ . The indices  $i; j$  label the operators and  $n$  the states. This product should have the same exponential behavior, i.e., the same mass, as the corresponding eigenvalue. Of course, they may differ in their amplitude since  $C_{ij}(t) \begin{smallmatrix} n \\ j \end{smallmatrix}$  gives the eigenvalue times some overlap factor. But much more important is the fact that these overlap factors ultimately provide us with the ratios of the amplitudes. To give a quantitative estimate for the ratio, we have to plot the ratio with respect to time. When the ratio has plateaued, we can be sure that higher excited states do not play a role anymore.

Local operators are well defined in the context of quantum field theory and therefore the ratio of their couplings is of particular interest. Furthermore, this will provide us with a clear answer if radial excitations have overlap with local hybrid operators. Figure 5 shows the ratio of the overlaps of the local hybrid and the local normal operator for the ground state and the first radial excitation. We clearly find that radial excitations have non-zero overlap with local hybrid operators. This is no big surprise since, after all, the radial excitations still have the same quantum numbers as the hybrid operators. In both cases, however, the coupling of the local normal operator to the state is about 90 times larger than the coupling of the local hybrid operator. Besides the nice quantitative estimate, we see from the left plot of Fig. 6 that the ratio for the first radial excitation is slightly below the one for the ground state. Finally the right plot of Fig. 6 shows the ratio of the couplings for the third

eigenstate, which we suppose to be the hybrid. We see that for the hybrid excitation the local hybrid operator has about the same weight as the local normal operator.

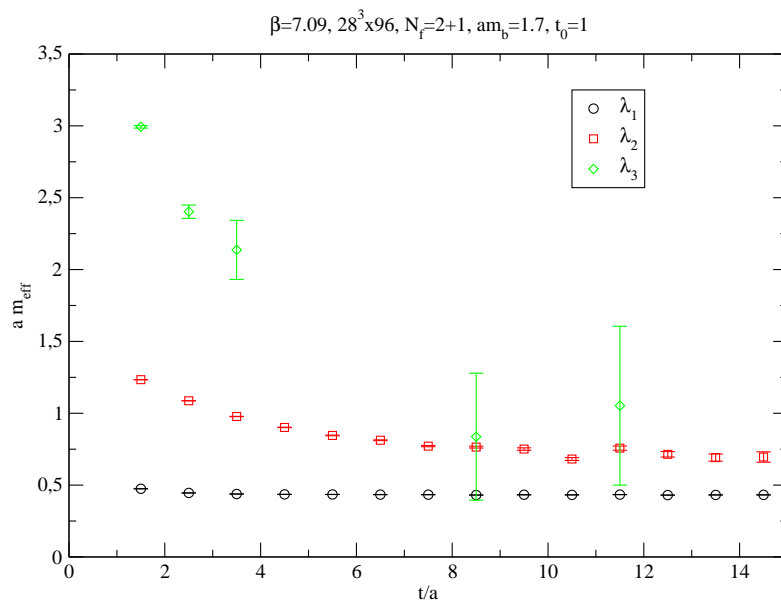


Fig. 4. Effective masses of the three eigenvalues in the basis  $N_{ll}(1), N_{nn}(2), H_{ll}(3)$  for the dynamical lattice with  $\beta = 7.09$  and  $am_b = 1.7$ .  $t_0$  is the normalization timeslice.

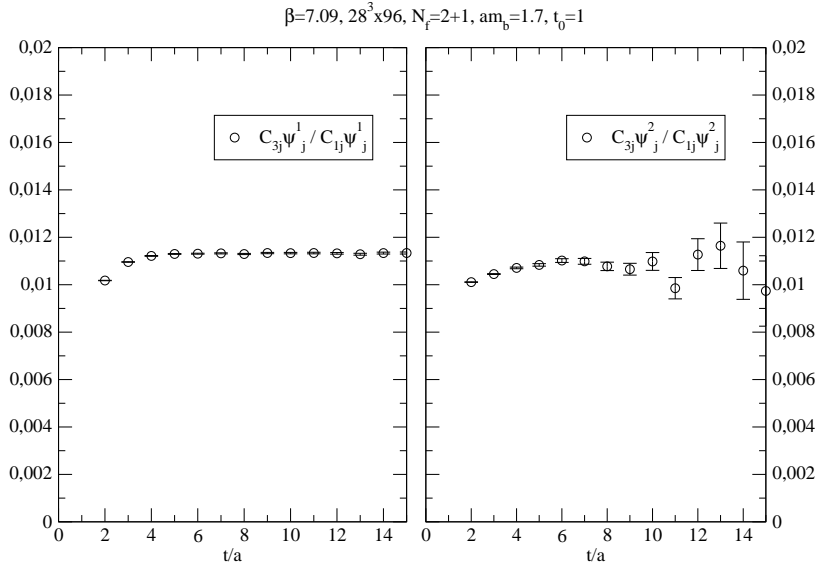


Fig. 5. The ratio of the couplings of the two local operators to the ground state is shown in the left plot, the same for the first excitation is in the right plot.

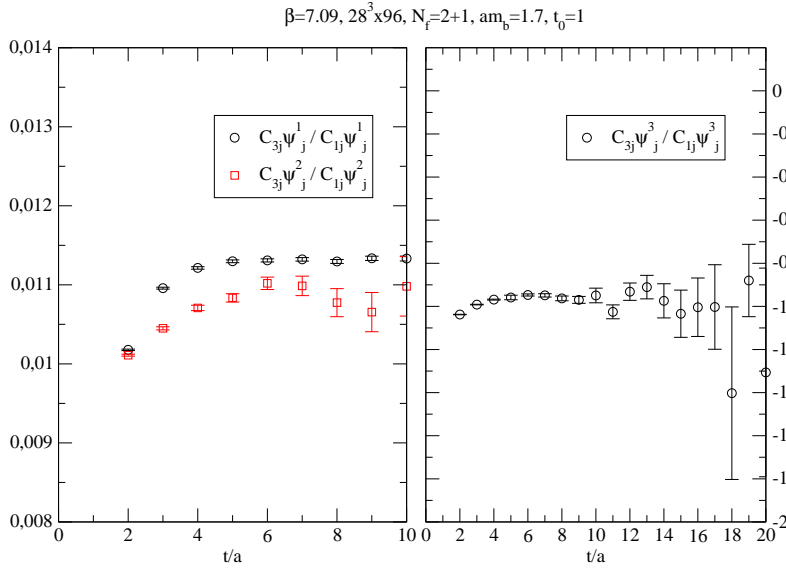


Fig. 6. The left plot shows the two ratios of Figure 5 zoomed in.  $\frac{h_{0,3} \beta_1}{h_{0,1} \beta_1}$  is shown in the right plot.

### 6.3 Enlarged basis

In order to obtain better signals from our correlators and to show a general feature of our operators, we increase the number of normal operators in the basis. The enlarged basis is built up from  $N_{ll}(1)$ ,  $N_{ln}(2)$ ,  $N_{nn}(3)$ ,  $N_{ww}(4)$ ,  $H_{ll}(5)$ . Figure 7 shows the effective masses of the eigenvalues. For this choice of basis we manage to obtain an acceptable signal even for the fourth state. The ratios of the couplings for the ground state, the first radial excitation and the hybrid excitation are shown in Fig. 8. Figure 9 shows the ratios for the third and fourth state, two further radial excitations which have been skipped in the previous basis. Again the results are close to those for the ground state and the first radial excitation.

A property of local operators reveals itself when we look again at the ratio of amplitudes. A comparison of the ground state and the first radial excitation ratio in two different bases is shown in Fig. 10. The explicit forms of the bases are: Basis 1 -  $N_{ll}(1)$ ,  $N_{ln}(2)$ ,  $N_{nn}(3)$ ,  $N_{ww}(4)$ ,  $H_{ll}(5)$ , basis 2 -  $N_{ll}(1)$ ,  $N_{ln}(2)$ ,  $N_{nn}(3)$ ,  $H_{ll}(4)$ ,  $H_{ln}(5)$ ,  $H_{nn}(6)$ . Even though, we change our basis by substituting smeared normal operators by other smeared ones, the ratios of the couplings of the local operators remain the same for these states. This implies that local operators are "approximately" orthogonal to smeared ones (i.e., they have very small overlap). If they would overlap significantly, adding a smeared operator to the basis would change the ratio, because the smeared operator could "steal" some contribution of the projection of the physical state onto the local operator. When looking at ratios of couplings of two smeared operators, we see that they change significantly when another smeared operator is added to, or removed from, the basis. That means that the smeared operators we use are not orthogonal to each other. Since the coupling ratio of the local operators stays the same in every arbitrary basis, as we found, we can also exclude that the smeared operators occasionally steal exactly the same contribution from the local normal and the local hybrid operator in such a way that the ratio remains the same. The result about the orthogonality of local and smeared operators is very plausible. The spatial width of the local operators is near zero and they have finite height. So their convolution with the Jacobi smeared operators should be quite small, as we found. The constancy of the ratio under the change of basis is an important justification for our conclusions. If this would not be the case, we would have less chance to determine the amplitudes for the local operators.

It is worth noting that including further operators in the basis does not help to improve the outcome; quite the contrary, they enhance the overlap with higher excited states or they contribute more noise than new information and thereby disrupt the signals.

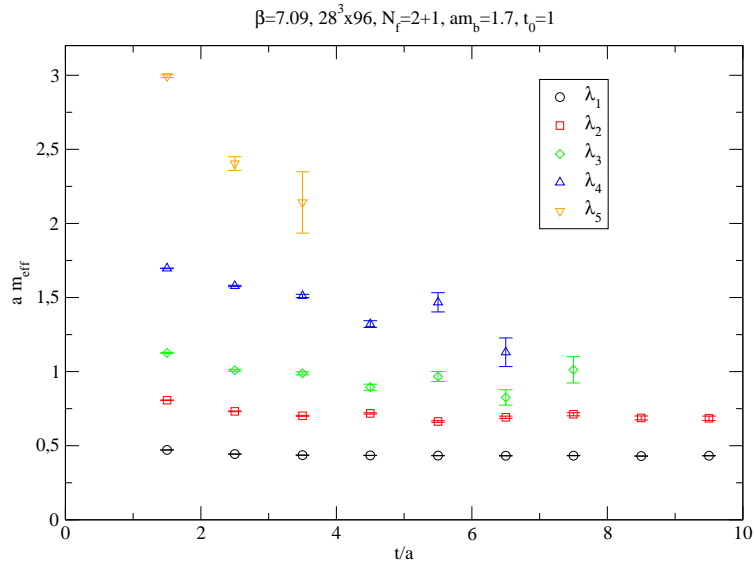


Fig. 7. Effective masses of the five eigenvalues in the basis  $N_{ll}(1)$ ,  $N_{ln}(2)$ ,  $N_{nn}(3)$ ,  $N_{ww}(4)$ ,  $H_{ll}(5)$  for the dynamical lattice with  $\beta = 7.09$  and  $am_b = 1.7$ .

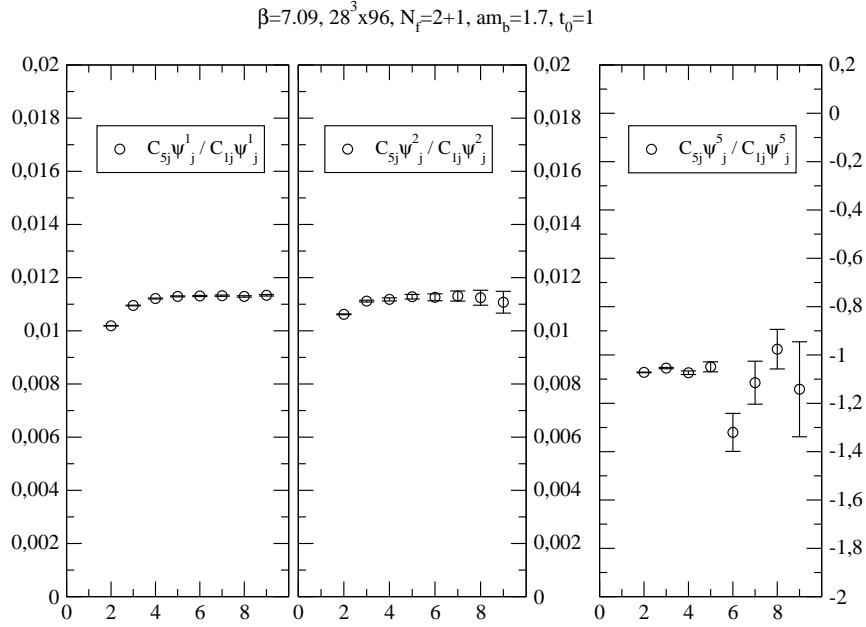


Fig. 8. The ratio of the couplings of the two local operators to the ground state, to the first radial excitation and to the hybrid. All in the new  $5 \times 5$  basis. Note the different scale for the hybrid excitation.

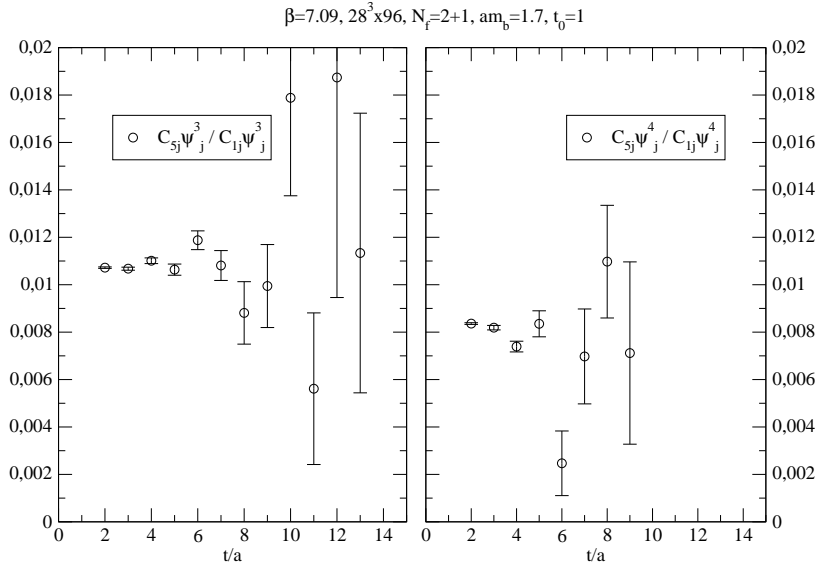


Fig. 9. The ratio of the couplings of the two local operators to the third state is shown in the left plot, the one for the fourth state is in the right plot. Both in the new 5 5 basis.

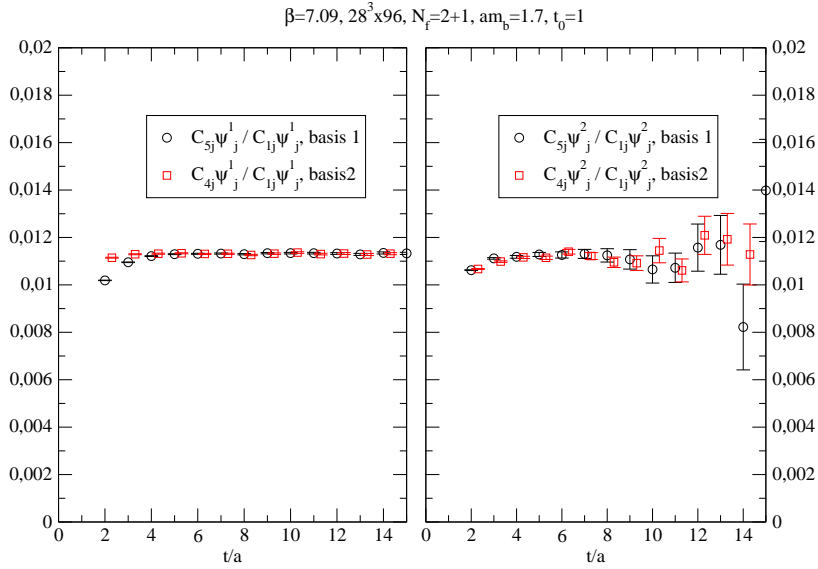


Fig. 10. The ratio of the couplings of the two local operators to the ground state is shown in the left plot, the one for the first excitation is in the right plot, both for two different sets of operators [basis 1 is  $N_{ll}(1), N_{ln}(2), N_{nn}(3), N_{ww}(4), H_{ll}(5)$  and basis 2  $N_{ll}(1), N_{ln}(2), N_{nn}(3), H_{ll}(4), H_{ln}(5), H_{nn}(6)$ ]. The datapoints for the second basis are shifted by 0.3 for the sake of clarity.

## 6.4 Scale dependence

So far we have not considered renormalization. Therefore, we are left with ratios of the couplings lattice regularized at a scale  $a^{-1}$ . Nevertheless, we can observe the size and the trend of the scale dependence by using lattices with different values for the lattice spacing.

The ratios of the couplings for the ground and first excited state for two different lattice spacings are shown in Fig. 11, where now  $a_{\text{coarse}} = 2 \cdot a_{\text{fine}}$  for the coarser lattice. A clear scale dependence is visible. For the coarser lattices, thus for a lower energy scale, the ratios for the non-hybrid states decrease, whereas for the hybrid it increases. Given that the hybrid operator (in the numerator of the ratio) is not strictly a local current, but rather extended over a  $2 \times 2$  clover, this strong scale dependence is not that surprising. Unfortunately, with only two different lattice spacings available (and the same extent of the hybrid operator in lattice units) and outstanding renormalization we cannot say anything more definitive about this.

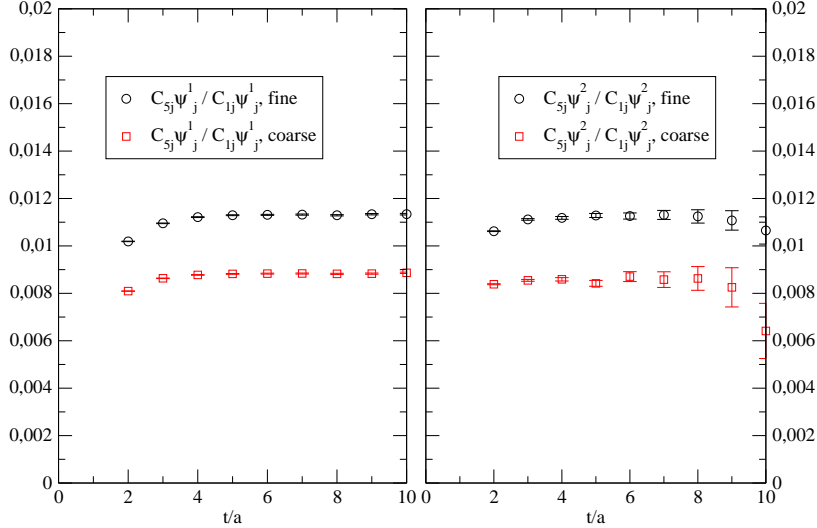


Fig. 11. The ratio of the couplings of the two local operators to the ground state is shown in the left plot, the one for the first excitation in the right plot. Each plot is for two different lattices with  $a^{-1} = 2101 \text{ MeV}$  (fine) and  $a^{-1} = 1497 \text{ MeV}$  (coarse).

## 6.5 Quenched/dynamical

Since we have quenched and unquenched (dynamical) lattices available, we can explore whether sea quark contributions affect the amplitudes. One would expect that they have influence at least for higher excited states which lie above the  $B\bar{B}$  threshold. If we take for the mass of the  $B$  meson  $5.3 \text{ GeV}$  and for the  $B$ -meson  $5.3 \text{ GeV}$ , the threshold is in lattice units about  $0.52$  above the lowest lying state on the dynamical  $\beta = 7.09$  lattice. Figure 12 shows the eigenstates in the basis  $N\bar{N}(1), N\bar{N}(2), N\bar{N}(3), N\bar{N}(4), H\bar{N}(5)$  for the  $N_f = 0$  lattice. The fact that the last two states are above the threshold and give better signals on the quenched lattice is maybe some indication for a decayed state on the dynamical configuration for large times. However, since the overlap of the operators we use with the decayed state is probably rather small, this remains as a speculation.

The ratios for both the dynamical and the quenched lattice are plotted together in Fig. 13. It is not clear if the slight change is really due to quenching effects. The slightly different scale of the two lattices (see Table 2) probably plays a greater role.

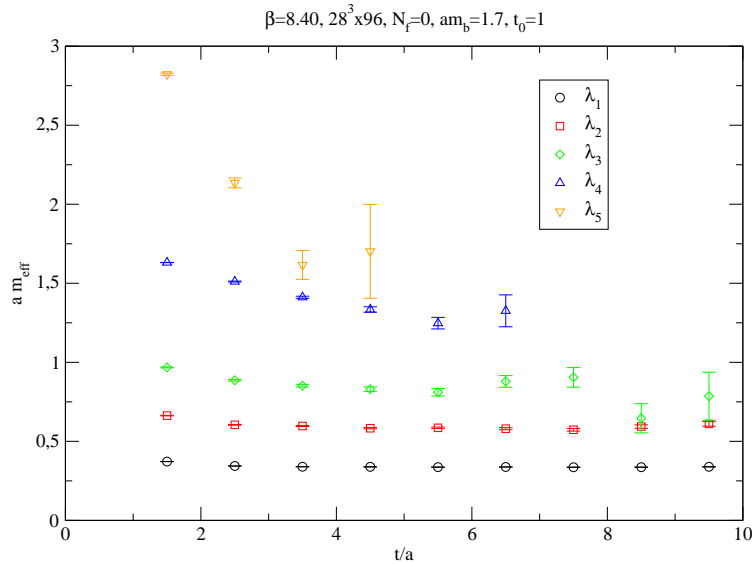


Fig. 12. Effective masses of the five eigenvalues in the basis  $N\bar{N}(1), N\bar{N}(2), N\bar{N}(3), N\bar{N}(4), H\bar{N}(5)$  for the quenched lattice with  $\beta = 8.40$  and  $am_b = 1.7$ .

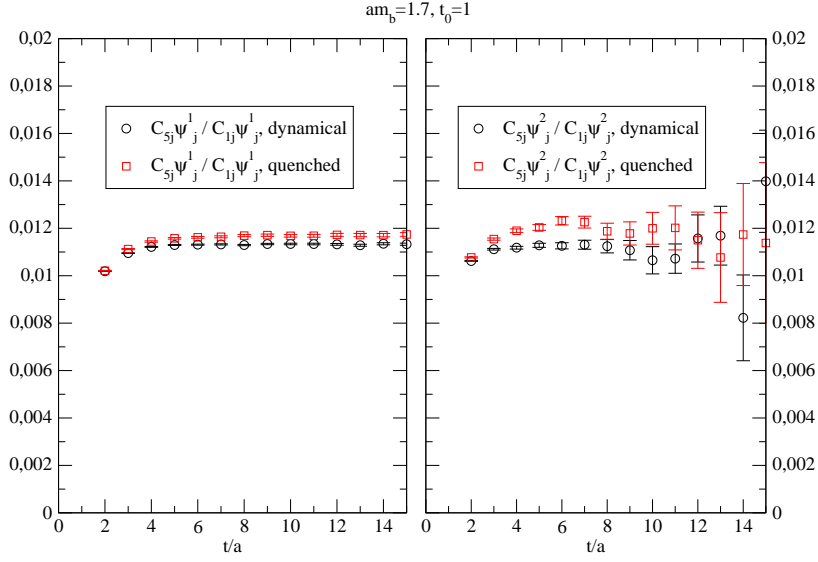


Fig. 13. The ratio of the couplings of the two local operators to the ground state is shown in the left plot, the one to the first excitation in the right plot. Both for the quenched ( $\beta = 8.40$ ) and the dynamical ( $\beta = 7.09$ ) lattices.

## 6.6 Further results

This section briefly covers the results for the  $\psi_0$ , which is, from an experimental viewpoint, less accessible, since its ground state has been observed in only one type of experiment and none of its excitations have been detected up to now.

Figure 14 shows the effective masses of the eigenvalues in the basis  $N_{ll}(1)$ ,  $N_{ln}(2)$ ,  $N_{nn}(3)$ ,  $N_{ww}(4)$ ,  $H_{ll}(5)$ . The local coupling ratios are plotted in Figure 15. Typically, the signals for pseudoscalars are slightly better than the ones for vectors. The increase of the ratio of the local couplings by about a factor three can be traced back to the fact that in the  $0^+$  hybrid operator all three components of the  $B$ -eld are included.

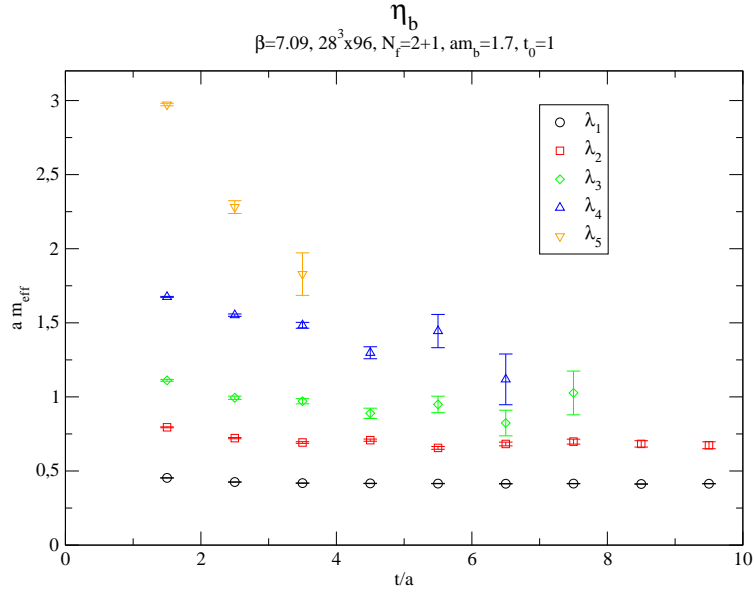


Fig. 14. Effective masses of the five eigenvalues in the basis  $N_{ll}(1)$ ,  $N_{ln}(2)$ ,  $N_{nn}(3)$ ,  $N_{ww}(4)$ ,  $H_{ll}(5)$  for the pseudoscalar on the dynamical lattice with  $\beta = 7.09$  and  $am_b = 1.7$ .

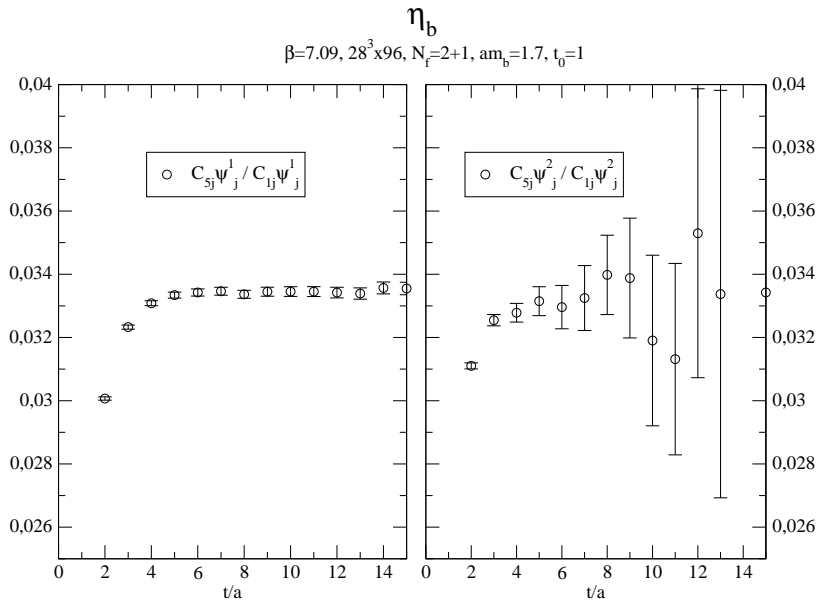


Fig. 15. The ratio of the couplings of the two local operators to the ground state is shown in the left plot, the one to the first excitation in the right plot. Both for the pseudoscalar state on the dynamical lattices.

As a crosscheck we also determined the couplings of the two local operators to the two lowest lying states by directly fitting a three by three correlator matrix. To do so, we build up a matrix of correlators with three different operators, namely  $N_{ll}(1)$ ,  $N_{nn}(2)$ ,  $H_{ll}(3)$ . Then we fit the matrix to the functional form

$$C_{ij}(t) = A_i^0 A_j^0 e^{-am_0 t} + A_i^1 A_j^1 e^{-am_1 t}; \quad i, j = 1, 2, 3; \quad (8)$$

where  $A_i^0$  is the coupling of the ground state to the  $i$ th operator and  $A_i^1$  is the coupling of the first excited state to the  $i$ th operator.

The fitting results for the couplings are given in Table 4. The time  $t$  range is 15 to 25. This range multiplied by the nine different operator combinations yields 90 degrees of freedom to determine eight parameters, namely six couplings and two masses. Within the errors the results are in good agreement with the ones from the variational method, for both the ground and the excited state the ratio of the couplings to the two local operators is again about 1/30 in the pseudoscalar channel.

parameter	value
$A_1^0$	0.189
$A_3^0$	0.00635 (2)
$A_1^1$	0.130 (14)
$A_3^1$	0.00435 (59)

Table 4  
Results for the fit of the correlator matrix.

## 7 Conclusions

In the end of this work we want to summarize our results and draw conclusions from them. We found, as do many others working on spectroscopy, that the variational method is a very promising approach since it allows one to clearly separate the individual mass eigenstates of the theory and, furthermore, to find out the ratio of the couplings of a state to different operators included in the basis of the cross correlator matrix. The low cost of simulations in the NRQCD framework also contributed to the success of our analysis.

Regardless of the choice of basis, we found the quite amazing fact that the ground state and all radial excitations of bottomonia have about the same ratio for their couplings to the two local operators we considered. One may interpret this as there being about the same suppression of gluonic content

at the origin of the wavefunctions for these states. For the hybrid excitation the ratio is largely enhanced in favor of the hybrid operator. The outcome for the radial excitation clearly contradicts the results of [1]. With inputs of single symmetric correlator runs we actually were able to conclude that in the correlator built from hybrid operators the amplitude of the radial excitation is down by  $O(100)$  compared to the hybrid excitation. The smallness of the coupling is the only reason why Liu and Luo were not able to see any radial excitation in their hybrid correlators.

Furthermore, we investigated the scale dependence of the local coupling ratios and found a clear dependence. However, a careful renormalization procedure is necessary to judge the physical relevance of this scale dependence. Quenching effects upon the ratios of couplings appeared to be small. Finally we gave results for the pseudoscalar channel and crosschecked the numbers obtained from the variational method by directly fitting a three by three cross correlator matrix.

Acknowledgements

We wish to thank Andreas Schafer for fostering a large research group, thereby making collaborations like this possible. We would also like to thank the MILC Collaboration for making their configurations publicly available. This work is supported by GSI.

References

- [1] X. Q. Luo and Y. Liu, Phys. Rev. D 74, 033002 (2006); Erratum *ibid.* D 74, 039902 (2006) [hep-lat/0512044].
- [2] C. M. d'Neile and C. Michael [UKQCD Collaboration], hep-lat/0607032.
- [3] C. Ehm ann, T. Burch and A. Schafer, PoS (LAT 2006)106 [arXiv:hep-lat/0609028].
- [4] T. Burch and D. Toussaint [MILC Collaboration], Hybrid configuration content of heavy S-wave mesons, Phys. Rev. D 68, 094504 (2003) [arXiv:hep-lat/0305008].
- [5] T. Burch, C. Gattringer, L. Y. Glozman, C. Hagen, C. B. Lang and A. Schafer, Phys. Rev. D 73, 094505 (2006) [arXiv:hep-lat/0601026].
- [6] C. Michael, Nucl. Phys. B 259 (1985) 58.
- [7] M. Luscher and U. Wol, Nucl. Phys. B 339 (1990) 222.

- [8] T. Burch, C. Gattringer, L. Y. Glozman, C. Hagen and C. B. Lang, Phys. Rev. D 73, 017502 (2006) [[arXiv:hep-lat/0511054](#)].
- [9] G. P. Lepage, L. Magnea, C. Nakhleh, U. Magnea and K. Hombostel, Phys. Rev. D 46, 4052 (1992) [[hep-lat/9205007](#)].
- [10] G. P. Lepage and P. B. Mackenzie, On The Viability Of Lattice Perturbation Theory Phys. Rev. D 48, 2250 (1993) [[arXiv:hep-lat/9209022](#)].
- [11] C. Aubin et al., Phys. Rev. D 70, 093005 (2004) [[hep-lat/0402030](#)].